Original Article

Circulating lung cancer exosomes damage the niche of intestinal stem cells

Ke Wang[1,2#], Lu Xu[2#], Jianhua Feng[1,2#], Shubin Wang[1,2#], Xi Wang[2], Junyi Zou[1], Zhenni Xu[2], Lingxiao Huang[2], Wenjun Jiang[2], Jin Zhou[1], Xudan Lei[2], Dengqun Liu[2]

[1]Department of Oncology, Sichuan Cancer Hospital & Institute, Sichuan Clinical Research Center for Cancer, Sichuan Cancer Center, School of Medicine, University of Electronic Science and Technology of China, Chengdu, China; [2]Radiation Oncology Key Laboratory of Sichuan Province, Department of Experimental Research, Sichuan Cancer Hospital & Institute, Sichuan Clinical Research Center for Cancer, Sichuan Cancer Center, School of Medicine, University of Electronic Science and Technology of China, Chengdu, China

Contributions: (I) Conception and design: D Liu, X Lei, J Zhou, K Wang; (II) Administrative support: L Huang, X Lei, D Liu; (III) Provision of study materials or patients: None; (IV) Collection and assembly of data: K Wang, L Xu, J Feng, S Wang, X Wang, Z Xu; (V) Data analysis and interpretation: K Wang, L Xu, J Feng, S Wang, Z Xu, D Liu; (VI) Manuscript writing: All authors; (VII) Final approval of manuscript: All authors.

[#]These authors contributed equally to this work.

Correspondence to: Jin Zhou, MD. Department of Oncology, Sichuan Cancer Hospital & Institute, Sichuan Clinical Research Center for Cancer, Sichuan Cancer Center, School of Medicine, University of Electronic Science and Technology of China, 55 South Renmin Road Section 4, Chengdu 610041, China. Email: zhoujin1@scszlyy.org.cn; Xudan Lei, PhD; Dengqun Liu, PhD. Radiation Oncology Key Laboratory of Sichuan Province, Department of Experimental Research, Sichuan Cancer Hospital & Institute, Sichuan Clinical Research Center for Cancer, Sichuan Cancer Center, School of Medicine, University of Electronic Science and Technology of China, 55 South Renmin Road Section 4, Chengdu 610041, China. Email: leixudan2020@126.com; dengqunliu@uestc.edu.cn.

Background: Cancer-associated weight loss occurs frequently in patients with advanced lung cancer. Many studies have demonstrated that tumor-derived exosomes could mediate the interplay between tumor cells and distal organs. In this study, we explored the interaction between lung cancer cell-derived exosomes (LCCDEs) and the niche of intestinal stem cells (ISCs).

Methods: Lewis lung carcinoma-1 (LLC1)-conditional medium (LLC1-CM), N,N'-Bis[5-(2,3-dihydro-1H-indol-1-yl)pentyl]-1,6-hexanediamine (GW4869)-conditional medium (GW4869-CM), LCCDEs and phosphate-buffered saline (PBS) were used to treat 6- to 8-week-old healthy male C57BL/6J mice (18–22 g) and B6.129P2-Lgr5$^{tm1(cre/ERT2)Cle}$/J (Lgr5-EGFP-IRES-creERT2) mice (Lgr5-EGFP mice). Additionally, enteroids were treated with LLC1-CM, A549 human lung adenocarcinoma cells (A549)-CM, LCCDEs of LLC1 cells and A549 cells and PBS. LCCDEs were characterized by transmission electron microscopy, Western blot, and nanoparticle tracking analysis. The influence of LCCDEs on intestine and ISCs was explored by hematoxylin & eosin staining, proliferation, differentiation, enteroid culture, and quantitative polymerase chain reaction. PKH26-labeled LCCDEs were detected in intestinal epithelial cell line 6 (IEC-6) cells and Lgr5-EGFP mice. The changes of ISCs' niche caused by LCCDEs were examined by p-S6, pERK1/2 and p-STAT3 immunostaining.

Results: LLC1-CM damaged the small intestines and small intestinal organoids. The inhibition of exosomes by GW4869 partially alleviated these effects. Purified LCCDEs altered the structure of the intestines, changed the proliferation and differentiation of ISCs and inhibited the growth of enteroids. In addition, PKH26-labeled LCCDEs entered the cytoplasm of IECs and Paneth cells and changed the messenger ribonucleic acid (mRNA) expression of many genes, including stem cell marker genes, growth factor genes, and epithelial marker genes. Mechanistically, LCCDEs decreased mTORC1 activity in Paneth cells and inhibited p-ERK1/2 signaling in ISCs.

Conclusions: We demonstrated that circulating exosomes derived from lung cancer could impair ISCs and alter their niche in mice, which further explained the interaction between lung cancer and the gastrointestinal tract. This study proposes a promising and novel therapy to overcome weight loss in patients

by decreasing LCCDEs secretion and blocking their binding to the intestine, which might be a feasible therapeutic approach in future clinical practice.

Keywords: Lung cancer; exosome; intestinal stem cell (ISC); Lgr5; microenvironment

Submitted Aug 26, 2024. Accepted for publication Jan 27, 2025. Published online Mar 10, 2025.
doi: 10.21037/tlcr-24-758
View this article at: https://dx.doi.org/10.21037/tlcr-24-758

Introduction

In clinical practice, many patients with advanced lung cancer experience malnutrition in the terminal stage, which is closely related to increased mortality and dysfunction of multiple organs (1). There are multiple reasons for this problem. According to the American Society of Clinical Oncology (ASCO) guidelines for cancer cachexia that were presented in 2020, the causes of cancer-associated cachexia (CAC) in affected patients include inappropriate dietary, disturbed dietary supplements, pharmacological side effects and insufficient exercise. Nutritional intervention is recommended in these guidelines as a reasonable strategy to improve nutritional condition (2). Malnutrition is an important factor that negatively affects the outcomes and quality of life of patients with advanced lung cancer.

Gastrointestinal (GI) tract is the major system responsible for food digestion and nutrient absorption. Moreover, GI symptoms and weight loss frequently occur in patients with adenocarcinoma and lung cancer (3). The intestinal epithelium is a frontline of nutrient absorption and innate immunity, and it is the most vigorously renewed tissue in mammals. Intestinal stem cells (ISCs) located within crypts provide numerous terminally differentiated epithelial cells to maintain the structural and functional integrity of the intestinal epithelium, but ISCs are sensitive to many harmful factors, such as infection, radiation, and aging (4-6). Meanwhile, ISCs reside in a niche composed of Paneth cells, macrophages, and myofibroblasts. The niche of ISCs is important for the physiological maintenance and damage-induced regeneration of ISCs (7,8). However, the influences of lung cancer and its secretory derivatives on ISCs have not been well investigated.

Exosomes are round extracellular vesicles (EVs) with diameters ranging from 40 to 160 nm, and they are encapsulated by a lipid bilayer membrane (9). Exosomes are produced in large amounts by cancer cells, and they can disseminate into the tumor microenvironment and then migrate into the blood and lymphatic circulation. Due to the complicated process of exosomes secretion, exosomes carry multiple constituents, including proteins, glycans, lipids, amino acids, DNA, ribonucleic acids (RNAs) [such as microRNAs (miRNAs), small interfering RNAs (siRNAs), and long non-coding RNAs (lncRNAs)], and cytosolic and cell-surface proteins (9,10). Depending on their cells of origin, exosomes may participate in different physiological or pathological processes. Tumor-derived exosomes can participate in interaction between tumor cells themselves, or between tumor cells and the microenvironment (11), or distal tissues and organs (12,13). Therefore, tumor cell-derived exosomes are important exocrine mediators through which tumor tissue affects the function of the whole body (14-16). Lung cancer cell-derived exosomes (LCCDEs) can regulate both the tumor microenvironment in the niche and distal organs by influencing intercellular communication and processes, such as immune cell evasion, angiogenesis and epithelial-mesenchymal transition (EMT) (17,18). As an important subtype of EVs, LCCDEs are taken up by other cells, with effects on cell phenotypes and cell-cell

Highlight box

Key findings

- This study reported the harmful influences of circulating lung cancer cell-derived exosomes (LCCDEs) on intestinal stem cells (ISCs) and their niche, including the decreased length of small intestine, the inhibition of enteroid formation. The mechanisms of LCCDEs induced intestinal damage included the inhibition of mTORC1 activity in Paneth cells and p-ERK1/2 signaling in ISCs.

What is known and what is new?

- Many lung cancer patients undergo weight loss and cancer associated cachexia.
- This study shows circulating LCCDEs could inhibit the function of ISCs and interrupt their residing microenvironments.

What is the implication, and what should change now?

- We should pay more attention to LCCDEs-induced dysfunction of gastrointestinal tract and develop novel therapy targeting the interaction between lung cancer and gut.

communication (19). Therefore, exosomes derived from Lewis lung carcinoma-1 (LLC1) were injected via tail vein of mice to mimic the exosomes produced by human lung adenocarcinoma and secreted into the bloodstream.

In this study, we aimed to explore the influence of LCCDEs on the epithelial integrity of the small intestine, especially the activity of ISCs and their niche, using histological methods and an organoid model. We found that LCCDEs could impair the proliferation and differentiation of ISCs and disrupt the balance of the ISCs' microenvironment, which caused pathological changes in the intestinal epithelium. We present this article in accordance with the ARRIVE reporting checklist (available at https://tlcr.amegroups.com/article/view/10.21037/tlcr-24-758/rc).

Methods

Mice

Six- to eight-week-old healthy male C57BL/6J mice (18–22 g) were obtained from Beijing HFK Bioscience Company. Upon arriving in our laboratory, the mice were acclimatized for one week. B6.129P2-Lgr5$^{tm1(cre/ERT2)Cle}$/J (Lgr5-EGFP-IRES-creERT2) mice were obtained from Jackson Laboratory. All the mice were kept in a specific pathogen-free (SPF) animal facility with free access to food and water. The animal experiments were conducted in accordance with the guidelines of the National Institutes of Health (NIH) "Guide for the Care and Use of Laboratory Animals (8th edition)", and all the experimental procedures were reviewed and approved by the Ethics Committee of Sichuan Cancer Hospital & Institute (No. SCCHEC-04-2023-01/8). A protocol was prepared before the study without registration.

Cell culture and collection of conditional mediums

The LLC1 cell line was purchased from the National Collection of Authenticated Cell Cultures (Shanghai, China). IEC-6 cells were obtained from the American Type Culture Collection (ATCC) and maintained in our laboratory. The cells were cultured in high-glucose Dulbecco's Modified Eagle Medium (DMEM) (HyClone, Utah, USA) supplemented with 10% fetal bovine serum (FBS) (Biological Industries, Haemek, Israel) and 1% penicillin/streptomycin solution (Beyotime, Shanghai, China). The cells were cultured in a CO_2 incubator (Thermo Fisher Scientific, Massachusetts, USA) with 5% CO_2 at 37 ℃. Cultured cells were digested with 0.25% trypsin containing 0.02% ethylenediaminetetraacetic acid (EDTA) (HyClone) before passaging. When the LLC1 cells reached 80% confluence, the medium was replaced with fresh complete medium. After 24 h of incubation, the LLC1 conditional medium (LLC1-CM) was collected, filtered through a 0.22 μm syringe filter, aliquoted and frozen at –20 ℃ before use. In addition, N,N'-Bis[5-(2,3-dihydro-1H-indol-1-yl)pentyl]-1,6-hexanediamine-conditional medium (GW4869-CM) was the conditional medium from LLC1 cells treated with 20 μM GW4849 for 24 h.

Preparation and preservation of LCCDEs

The preparation of LCCDEs from LLC1 cells and A549 cells was conducted following a previously described method (20). Briefly, LLC1 cells and A549 cells were cultured in T75 flasks. When the cells reached 80% confluence, the medium was changed to fresh DMEM and Roswell Park Memorial Institute (RPMI)1640 containing 10% exosome-free FBS (Viva Cell, Shanghai, China). The cells were subsequently cultured in exosome-free medium for 24 hours. Afterward, the culture medium was collected, and the cellular debris was removed by centrifugation at 300 g for 15 min and 2,000 g for 15 min. After the first centrifugation step, the supernatant containing exosomes were obtained. Then, the supernatant was transferred to a 35 mL ultracentrifugation tube and centrifuged at 10,000 g and 4 ℃ for 30 min, after which the centrifuge tubes were washed with 5 mL of phosphate-buffered saline (PBS) and centrifuged at 120,000 g for 70 min at 4 ℃ to collect LCCDEs. LCCDEs were subsequently resuspended in 200 μL of ice-cold PBS (21). LCCDEs were characterized before use. The concentration of LCCDEs was determined with a BCA kit, and the LCCDEs were preserved in an Ultra-Low Freezer at –80 ℃ (22,23).

Characterization of exosomes

Exosomes were identified by transmission electron microscopy (TEM), Western blot (WB), and nanoparticle tracking analysis (NTA). The morphology of LCCDEs was examined under an electron microscope (JEOL, Tokyo, Japan). The protein concentration of LCCDEs was determined with a BCA kit (Bosterbio, Wuhan, China). For WB, 4.5 nm PVDF membranes were blocked in 3% bovine serum albumin (BSA) for 50 min at room temperature. CD63 was used as a marker of exosomes for WB. A polyclonal rabbit anti-CD63 antibody (SAB4301607;

Sigma, St. Louis, USA) was diluted 1:1,000 and incubated overnight. Horseradish peroxidase (HRP)-labeled goat anti-rabbit IgG (1:10,000, A0168, Sigma) was used to visualize the CD63 band. NTA was used to determine the diameter and size distribution of LCCDEs.

Treatment of mice and tissue collection

All mice were divided into different groups by random number method. In the conditional medium experiment, mice were injected with 200 µL of LLC1-CM or PBS per mouse via the tail vein for 5 consecutive days. In the GW4869 experiment, mice were treated with LLC1-CM or GW4869-CM. In the exosome experiment, the mice were treated with LCCDEs via tail vein injection. The doses of LCCDEs were 1.25 and 2.5 mg/kg/d per mouse, and the treatment was administered for five continuous days. Mice in the control group were treated with the same volume of PBS without LCCDEs. Lgr5-EGFP mice were injected with PKH26-labeled LCCDEs and sacrificed for frozen sectioning after 6 hours. At the end of treatment with LCC1-CM or LCCDEs, the mice were injected with 100 mg/kg BrdU for 90 min to label proliferative crypt epithelial cells and sacrificed by cervical dislocation. The intestines were quickly removed, and gross images of the GI tract were captured. Then, the intestines were fixed in 4% paraformaldehyde (PFA) overnight and subjected to regular tissue processing following our laboratory protocols. In this study, *n* referred to number of animals, each group contained 3–5 mice and mice were fed in separate cages, with three slices obtained from each experimental animal used for data analysis. To minimize potential confounders, such as the order of treatments and measurements, we randomized the sequence of treatments and measurements across animals. Additionally, cages were rotated regularly to control for environmental factors like light and temperature variations due to cage location. The experimenters and data analysts were blinded to the group allocation of the mice to further reduce bias.

5'-ethynyl-2'-deoxyuridine (EdU) assay

A BeyoClick™ EdU-555 Cell Proliferation Kit (Beyotime) was used to evaluate the proliferation of IEC-6 cells. Briefly, IEC-6 cells were seeded in 96-well plates overnight. When the IEC-6 cells had completely adhered to the bottom of the plate, fresh complete DMEM containing 25% (v/v) LLC1-CM was added to the wells of the experimental group, and no LLC1-CM was added for the control group. The cells were further cultured for another 24 h. Afterward, EdU was added to all the wells at a final concentration of 1 mM, and the cells were incubated for 2 h. Finally, the IEC-6 cells were fixed with 4% PFA at room temperature for 30 min and washed with PBS. EdU staining was conducted following the manufacturer's protocol. Nuclei were stained with 4',6-diamidino-2-phenylindole (DAPI) solution. Images were captured with a Leica SP5 confocal microscope.

Histological analysis and immunostaining

Intestinal blocks were sectioned into 4 µm thick sections. The sections were stained with hematoxylin & eosin (H&E). Immunohistochemistry (IHC) was conducted as previously described. Briefly, paraffin slides were deparaffinized in xylene and gradient ethanol, and antigen retrieval was performed in Tris-EDTA buffer (pH =9) at 100 ℃ for 20 min. Primary antibodies in blocking buffer were used at a dilution of 1:200, including mouse anti-BrdU, rabbit anti-Olmf4, rabbit anti-cleaved-caspase-3, rabbit anti-pERK1/2, and rabbit anti-p-STAT3 antibodies. The slides were incubated overnight at 4 ℃. Afterward, the tissues were thoroughly washed with PBS and incubated with the appropriate secondary antibodies for 40 min. 3,3'-diaminobenzidine (DAB) solution was used to visualize positive signals. Finally, the IHC slides were mounted with neutral balsam. For immunofluorescence staining, tissues were incubated with rabbit anti-phospho-S6 ribosomal protein (Ser240/244, p-S6) and goat anti-lysozyme antibodies overnight, and then Alexa Fluor™ 488 donkey anti-rabbit IgG and Alexa Fluor™ 594 donkey anti-goat IgG (Thermo Fisher, Massachusetts, USA) were used to identify cells positive for staining. Nuclei were counterstained with DAPI, and the slides were mounted with anti-fade fluorescence mounting medium.

Alcian blue staining and periodic acid-Schiff (PAS) staining

Alcian blue and PAS staining was used to visualize Paneth cells and goblet cells, which are important for maintaining homeostasis of the intestinal epithelium. Rehydrated slides were prepared as described above. The slides were stained with Alcian blue staining solution (Sangon, Shanghai, China) for 15 minutes. Then, the slides were washed and counterstained with nuclear fast red for 5 minutes. PAS staining was performed with a commercial kit (Solarbio,

Beijing, China) following the manufacturer's protocols. The slides were counterstained with hematoxylin before mounting.

Enteroid culture

Small intestinal crypts were freshly isolated as described previously (7). Briefly, 5–8 cm of jejunal tissues were removed, flushed with cold PBS and opened longitudinally on ice. The tissues were then cut into 3–5 mm pieces with scissors. The jejunal segments were washed briefly with cold PBS and then placed in ice-cold PBS supplemented with 2 mM ethylenediaminetetraacetic acid (EDTA) (Invitrogen, California, USA). The tissue was incubated for 30 min on ice and then washed with PBS. Villi and crypts were separated from the lamina propria by vigorous shaking, and the crypts were purified via passage through a 70-μm strainer. Individual crypts were collected by centrifugation at 4 ℃ and 1,000 ×g for 3 min. Finally, the crypts were resuspended in Matrigel (Corning, New York, USA) and seeded in 96-well flat-bottom plates (100 crypts/well). The plates were incubated at 37 ℃ for 10 min, after which IntestiCult™ OGM (StemCell Technologies, Vancouver, Canada) supplemented with 1× penicillin/streptomycin (Beyotime) was added to the plates. The culture medium was replaced every 3 days.

Treatment of enteroids

After 6 hours of culture at 37 ℃ with 5% CO_2, the intestinal enteroids were treated with LLC1-CM and A549-CM or LCCDEs of LLC1 cells and A549 cells. LLC1-CM and A549-CM was added to the culture medium at percentages of 25% (v/v) and 50% (v/v), respectively. The GW4869-CM group was treated with IntestiCult OGM supplemented with 50% (v/v) LLC1-CM and pretreated with 20 μM GW4869 for 24 h. To evaluate the influence of exosomes from LLC1 cells and A549 cells on small intestinal enteroids, enteroids were treated with different concentrations of LCCDEs, including 50, 100 and 200 μg/mL. The growth characteristics of the enteroids were observed every day. All enteroid quantifications were conducted by three different researchers on the first day and the third day after LCCDEs treatment.

Image capture and processing

Images of H&E-stained slides and IHC-stained sections were captured with an Olympus BX51 microscope. Immunofluorescent images were captured with an A1R Nikon confocal microscope (Nikon, Tokyo, Japan) or Leica SP5 confocal microcope. Enteroids were observed and imaged with an M5000 (ThermoFisher) or Cytation 5 (BioTek, Vermont, USA) system. The characteristics of the intestinal villi and crypts were evaluated with ImageJ software (NIH, Maryland, USA). Images of the slides and sections were edited with Adobe Photoshop and Adobe Illustrator.

Quantitative polymerase chain reaction (qPCR) assay

Total RNA was extracted from small intestines using TRIzol reagent (Ambion, Texas, USA) following the manufacturer's protocol. First-strand cDNA was amplified from 1 μg of RNA. The relative mRNA expression levels of different genes were quantified with Hieff qPCR SYBR Green Master Mix reagent (Yeasen, Shanghai, China), normalized to β-actin expression, and calculated via the $2^{-\Delta\Delta Ct}$ method. Quantitative real-time PCR was performed on a Bio-Rad iQ5 System. The primers used for qPCR were synthesized by BGI Genomics (Beijing, China). The specific primer sequences used for the target genes were listed in *Table 1*.

Statistical analysis

All the statistical analyses were performed with GraphPad Prism 9.4.1 (GraphPad, San Diego, CA, USA) and ImageJ 1.52q software. The data were presented as the mean ± standard deviation (SD). Statistical significance was evaluated using Student's *t*-test for comparisons between two groups, and we applied the Kruskal-Wallis *H* test for comparisons among three or more groups and the Mann-Whitney *U* test for pairwise comparisons. P values less than 0.05 were considered to indicate statistical significance.

Results

Medium of lung cancer cells impaired morphology and proliferation in the small intestine

In this study, mice were first treated with LLC1-CM for five consecutive days via tail vein injection. The length of the small intestine was substantially decreased in the LLC1-CM group than in the control group (34.07±1.17 *vs.* 28.53±3.18 cm) (*Figure 1A*). Statistical analysis revealed a significant difference between these two groups (*Figure 1B*). Since there were many nonepithelial cells present in the small intestine *in vivo*, we also examined how LLC1-CM

Table 1 Primer sequences used for qRT-PCR experiments

Gene	Forward	Reverse
Lgr5	CTCCCAGGTCTGGTGTGTTG	GAGGTCTAGGTAGGAGGTGAAG
Olmf4	CAGCCACTTTCCAATTTCACTG	GCTGGACATACTCCTTCACCTTA
Bmi1	ATCCCCACTTAATGTGTGTCCT	CTTGCTGGTCTCCAAGTAACG
Mki-67	ATCATTGACCGCTCCTTTAGGT	GCTCGCCTTGATGGTTCCT
IL-1β	ACCTCACAAGCAGAGCACAA	TTGGCCGAGGACTAAGGAGT
Wnt3	TGGAACTGTACCACCATAGATGAC	ACACCAGCCGAGGCGATG
Mist1	GCTGACCGCCACCATACTTAC	TGTGTAGAGTAGCGTTGCAGG
Lyz-1	ATGGAATGGCTGGCTACTATGG	ACCAGTATCGGCTATTGATCTGA
CHGA	ATCCTCTCTATCCTGCGACAC	GGGCTCTGGTTCTCAAACACT
Muc2	AGGGCTCGGAACTCCAGAAA	CCAGGGAATCGGTAGACATCG
Actb	GGCTGTATTCCCCTCCATCG	CCAGTTGGTAACAATGCCATGT

qRT-PCR, quantitative reverse transcription polymerase chain reaction; *Lgr5*, Leucine rich repeat containing G protein coupled receptor 5; *Omlf4*, olfactomedin 4; *Bmi1*, B cell-specific Moloney murine leukemia virus integration site 1; *Mki67*, marker of proliferation Ki-67; *IL-1β*, interleukin1 beta; *Wnt3*, wingless-type MMTV integration site family, member 3; *Mist1*, basic helix-loop-helix family, member a15; *Lyz-1*, Lysozyme 1; *CHGA*, chromogranin A; *Muc2*, mucin2, oligomeric mucus/gel-forming; *Actb*, beta actin.

affected the growth of intestinal epithelial cells (IECs) *in vitro* using IEC-6 cells. EdU incorporation assays showed that the administration of LLC1-CM significantly increased the number of EdU^+ IEC-6 cells (15±2.58 *vs.* 30±6.96) (*Figure 1C,1D*). In addition, LLC1-CM decreased enteroid formation in a dose-dependent manner both at the first day and the third day after treatment (*Figure 1E,1F*, Figure S1A,S1B), but it had no significant effect on the differentiation of enteroids (Figure S1A,S1C). Similarly, the enteroids treated by A549-CM showed a similar pattern as well (Figure S1D-S1H). Therefore, these results demonstrated that the medium of lung cancer cells could impair the morphology of the small intestine and affect cellular proliferation and enteroid formation, indicating that LLC1-CM could inhibit the activity of ISCs.

GW4869 alleviated the intestinal damage caused by LLC1-CM

As demonstrated above, LLC1-CM affects the structure of the intestines. Thus, we inferred that exosomes from LLC1-CM might be responsible for this impairment. We prepared LLC1-CM and GW4869-CM, and mice were then treated with these two conditional mediums for 5 consecutive days. Interestingly, the length of the small intestine in the GW4869-CM group was much greater than that in the LLC1-CM group (*Figure 2A,2B*), indicating that removal of exosome by GW4869 alleviated the impairment of LLC1-CM in the small intestine. We also examined the influence of GW4869 on the growth of LLC1 cells and found that GW4869 did not inhibit the growth of LLC1 cells, indicating that GW4869 inhibited the secretion of exosomes without impairing the viability of LLC1 cells (*Figure 2C,2D*). Afterward, we repeated the enteroid experiments. The crypts in the GW4869-CM group formed more enteroids at 24 h than did those in the LLC1-CM group (*Figure 2E,2F*). Moreover, we examined the characteristics of purified LCCDEs, and we found that LCCDEs expressed CD63, which is a classic marker of exosomes, and they had the typical appearance and diameter of exosome (*Figure 2G-2J*). Therefore, the results of these experiments supported the idea that the exosomes in LLC1-CM were the major components that impaired the health of small intestines.

LCCDEs impaired body weight and disrupted the intestinal structure

Since LLC1-CM had negative effects on the intestinal health of mice, we further treated the mice with purified LCCDEs (*Figure 3A*). Interestingly, compared with those in the control group, the mice in 2.5 mg/kg/d LCCDEs group began to lose weight on day 3, and there was a significant decrease in weight on days 4 and 5 (*Figure 3B*). More importantly, we found that 2.5 mg/kg/d LCCDEs dramatically reduced the length of the small intestine after

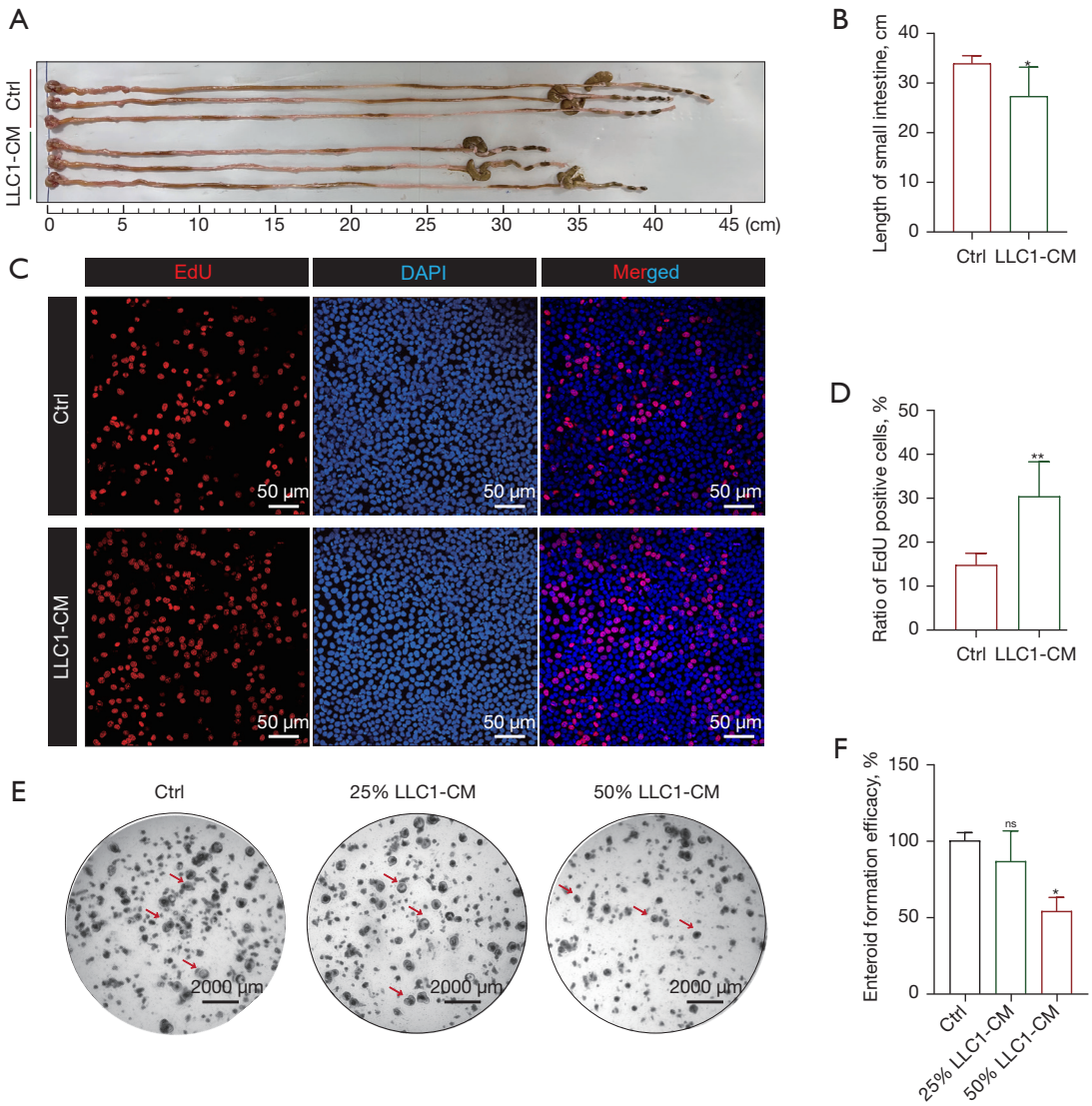

Figure 1 LLC1-CM impaired the morphology and proliferation of small intestines *in vivo* and *in vitro*. (A) The gross appearance of small intestines from control group and LLC1-CM group. (B) The length of small intestines in LLC1-CM group was significantly decreased compared with control group (n=3 per group). (C) IEC-6 cells were stained with EdU (red fluorescence) using a BeyoClick™ EdU-555 cell proliferation kit (Beyotime) to show those proliferating cells, and cell nuclei were counterstained with DAPI (blue fluorescence) (bar =50 μm). (D) The percentage of EdU$^+$ IEC-6 cell was significantly increased after the treatment by LLC1-CM for 24 h (n=3 wells per group). (E) Representative images of enteroids in control group and different LLC1-CM groups after 24 h culture (bar =200 μm). The red arrows indicated representative enteroids at this time. (F) Normalized enteroid formation efficacy at 24 h in different groups (n=4 wells each group). *, P<0.05; **, P<0.01; ns, not significant. LLC1-CM, Lewis lung carcinoma cell conditional medium; IEC-6, intestinal epithelial cell line 6; EdU, 5'-ethynyl-2'-deoxyuridine; DAPI, 4',6-diamidino-2-phenylindole.

five consecutive days of injections (*Figure 3C,3D*). However, the quantitative results demonstrated that the height of villi increased after the administration of LCCDEs (*Figure 3E,3F*). The mean depth and width of crypts also increased after the injection of LCCDEs (*Figure 3G,3H*). In summary, our results suggested that LCCDEs was able to decrease the body weight of mice *in vivo*, although there were increases in some structural parameters of the small intestine.

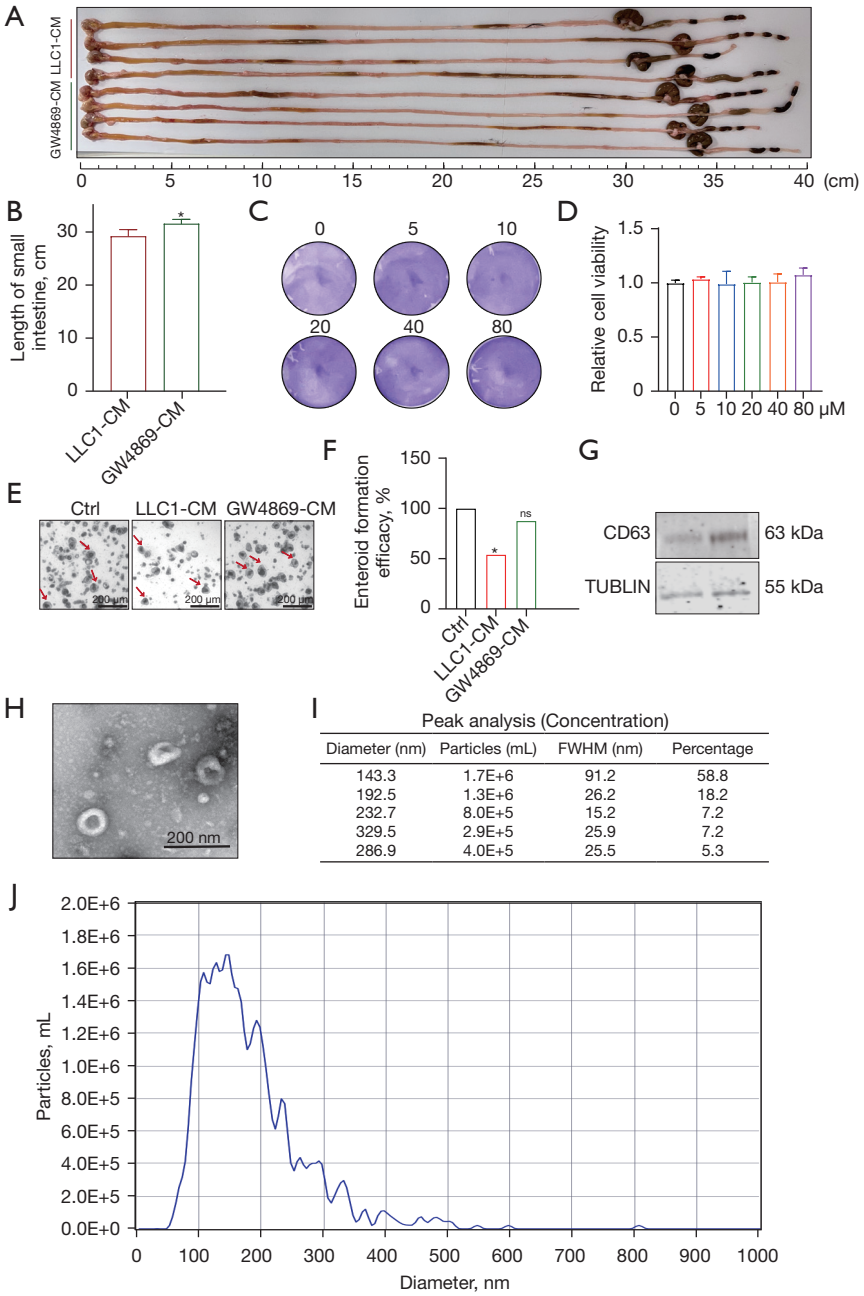

Figure 2 GW4869-CM abolished the impairment of small intestines caused by LLC1-CM. (A) Representative appearance of small intestines treated by LLC1-CM and GW4869-CM. (B) The length of small intestine in GW4869-CM group was increased compared with LLC1-CM (n=4 per group). (C) The crystal violet staining of LLC1 treated by different concentrations (0, 5, 10, 20, 40, 80 μM) of GW4869. (D) Quantification of cell proliferation ability of LLC1 cells treated by GW4869 (n=4 wells each group). (E) The representative images of enteroids treated by LLC1-CM and GW4869-CM after 24-hour culturing (bar =200 μm). Red arrows indicated representative enteroids at this time. (F) Enteroid formation efficacy in GW4869-CM group was increased compared with LLC1-CM group (n=4 wells per group). (G) CD63 was examined by Western blot to confirm the purification of LCCDEs. (H) The representative image of LCCDEs under electron microscope. (I,J) Diameter characteristics of LCCDEs were analyzed by NTA. *, P<0.05; ns, not significant. GW4869-CM, GW4869-conditional medium. LLC1-CM, Lewis lung carcinoma-1-conditional medium; LLC1, Lewis lung carcinoma-1; NTA, nanoparticle tracking analysis; FWHM, full width at half maximum.

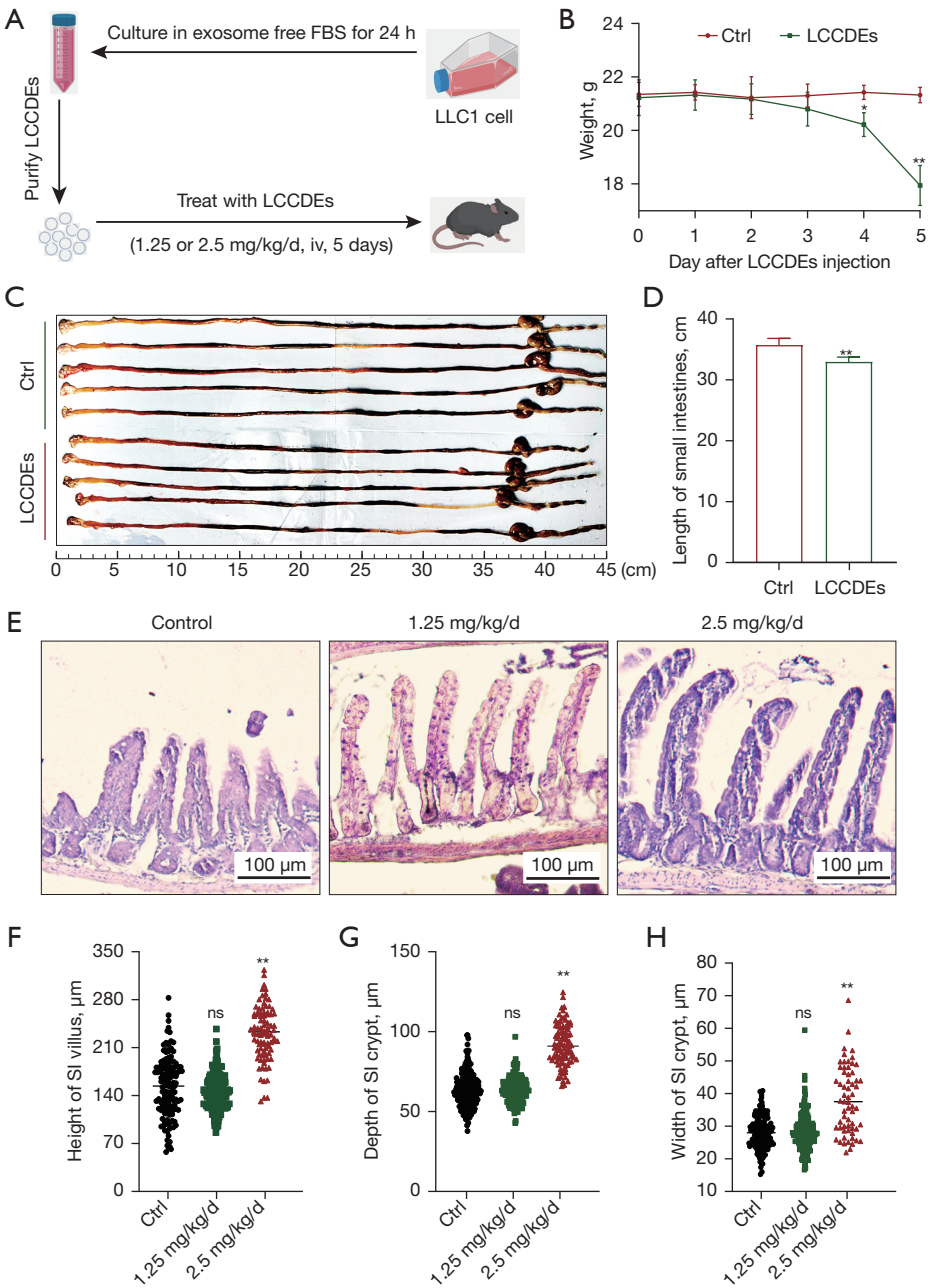

Figure 3 LCCDEs caused loss of body weight and changed the morphological characteristics of small intestines. (A) Schematic flowchart for isolation and administration of LCCDEs *in vivo*. (B) The average weight of mice was significantly decreased after the administration of LCCDEs (2.5 mg/kg/d, n=5 per group). (C) The representative gross images of gastrointestinal tract in control group and LCCDEs groups. (D) LCCDEs treatment dramatically decreased the length of small intestines (2.5 mg/kg/d, n=5 per group). (E) Representative H&E images of small intestinal tissues in different groups (bar =100 μm). (F) Comparison of average villous heights (n=5 mice per group). (G) Comparison of cryptal depth in different groups (n=5 mice per group). (H) The comparison of cryptal width of small intestine crypts (n=5 mice per group). *, P<0.05; **, P<0.01; ns, not significant. LCCDEs, lung cancer cell derived exosomes; H&E, hematoxylin & eosin; FBS, fetal bovine serum; LLC1, Lewis lung carcinoma-1; iv, intravenous; SI, small intestine.

LCCDEs changed the pattern of proliferation and differentiation of ISCs

Due to the above differences in body weight, intestinal length and structure observed after LCCDEs treatment, we further explored cellular dynamics in response to LCCDEs. First, apoptosis was evaluated by IHC staining for cleaved-caspase-3. There were more cleaved-caspase-3-positive apoptotic cells in the villi after the administration of LCCDEs (*Figure 4A*). Interestingly, the quantity of BrdU-positive proliferating cells was also significantly greater within intestinal crypts (*Figure 4B*,*4C*). Importantly, we stained ISCs with Olfm4, which is a widely used marker of ISCs. The number of Olfm4$^+$ ISCs decreased after LCCDEs treatment (*Figure 4D*,*4E*). In addition, we found that there were more Alcian blue$^+$ and PAS$^+$ goblet cells in the villous epithelium after LCCDEs treatment (*Figure 4F-4I*). The number of Alcian blue$^+$ cells within the crypts was gradually decreased with increasing doses of LCCDEs, while the quantity of PAS$^+$ cells was not changed siginificantly (*Figure 4F*,*4H*,*4J*,*4K*). Therefore, these data suggested that the administration of LCCDEs greatly impaired ISCs and altered their niche, with effects on the proliferation and differentiation patterns of ISCs.

LCCDEs inhibited the formation and growth of small intestinal organoids

Although LCCDEs significantly decreased the number of Olfm4$^+$ ISCs *in vivo*, we wondered whether LCCDEs could directly affect the activity of ISCs *in vitro*. The enteroids (intestinal organoids) were "mini guts" cultured *in vitro* containing ISCs and their differentiated epithelial cells. Since there were no mesenchymal cells in the enteroids, they could be used to directly observe the biological influence of LCCDEs on ISCs. LCCDEs were extracted and determined to be at a concentration of 1 μg/μL with a BCA kit. LCCDEs of LLC1 and A549 decreased in the efficacy of enteroid formation at day 1 and day 3 after the treatment with LCCDEs, and this decrease was concentration dependent, which indicated that a higher concentration of LCCDEs was accompanied by greater impairment of small intestinal organoid proliferation (*Figure 5A-5D*, Figure S2A,S2B). The impairment of small intestinal organoid proliferation persisted and could not be rescued quickly. However, the budding capacity of the small intestinal organoids was not affected by LCCDEs, even though the number of enteroids significantly decreased (*Figure 5E*,*5F*, Figure S2C-S2F). Taken together, these *in vitro* observations suggested that LCCDEs inhibited small intestinal organoid proliferation in a dose-dependent manner, but no difference in differentiation was observed.

LCCDEs negatively reshaped the niche of ISCs

Considering the above results, we further explored whether LCCDEs could be absorbed by IECs and how they changed the niche of ISCs. We used PKH26 to label LCCDEs and found that PKH26-positive LCCDEs could be absorbed by IEC-6 cells (*Figure 6A*,*6B*). Moreover, we treated Lgr5-EGFP mice and their enteroids with PKH26-labeled LCCDEs. PKH26-positive LCCDEs could be absorbed by enteroids (*Figure 6C*) and Paneth cells, which were intermingled between Lgr5-EGFP$^+$ ISCs (*Figure 6D*). Quantitative real-time PCR showed that LCCDEs treatment substantially changed the mRNA levels of many important genes. For example, LCCDEs significantly decreased the expression levels of *Lgr5* and *Olfm4* (marker genes of active ISCs), but they did not influence the mRNA expression of *Bmi1* (a marker of quiescent ISCs) (*Figure 6E-6G*). The expression of *Mki67*, a cellular proliferation marker, was increased (*Figure 6H*), which was consistent with the findings of IHC staining of BrdU in *Figure 4B*. The microenvironment-related genes (*IL-1*, *Wnt3*, and *Mist1*) and secretory lineage marker genes (*Lyz1*, *Chga*, and *Muc-2*) were also changed (*Figure 6I-6N*) (24,25). In addition, we stained p-S6 to examine mTORC1 activity and found that LCCDEs-treated mice had fewer p-S6-positive Paneth cells (*Figure 7A*,*7B*). Meanwhile, the numbers of p-ERK1/2-positive and p-STAT3-positive cryptal cells were also substantially decreased after the administration of LCCDEs (*Figure 7C-7F*). These findings indicated that circulating LCCDEs could be absorbed by IECs, and negatively affected the niche-related signaling pathways of ISCs.

Discussion

Lung cancer is the most frequent type of cancer, and it has a high mortality rate worldwide. Many lung cancer patients experience GI symptoms. In the present study, we demonstrated that LCCDEs reduced the body weight of mice and the lengths of the small intestines. Moreover, LCCDEs could impair the homeostasis of ISCs and their niche, as shown by decreased Olmf4$^+$ ISCs abundance, poor formation of enteroids, and altered mRNA expression of

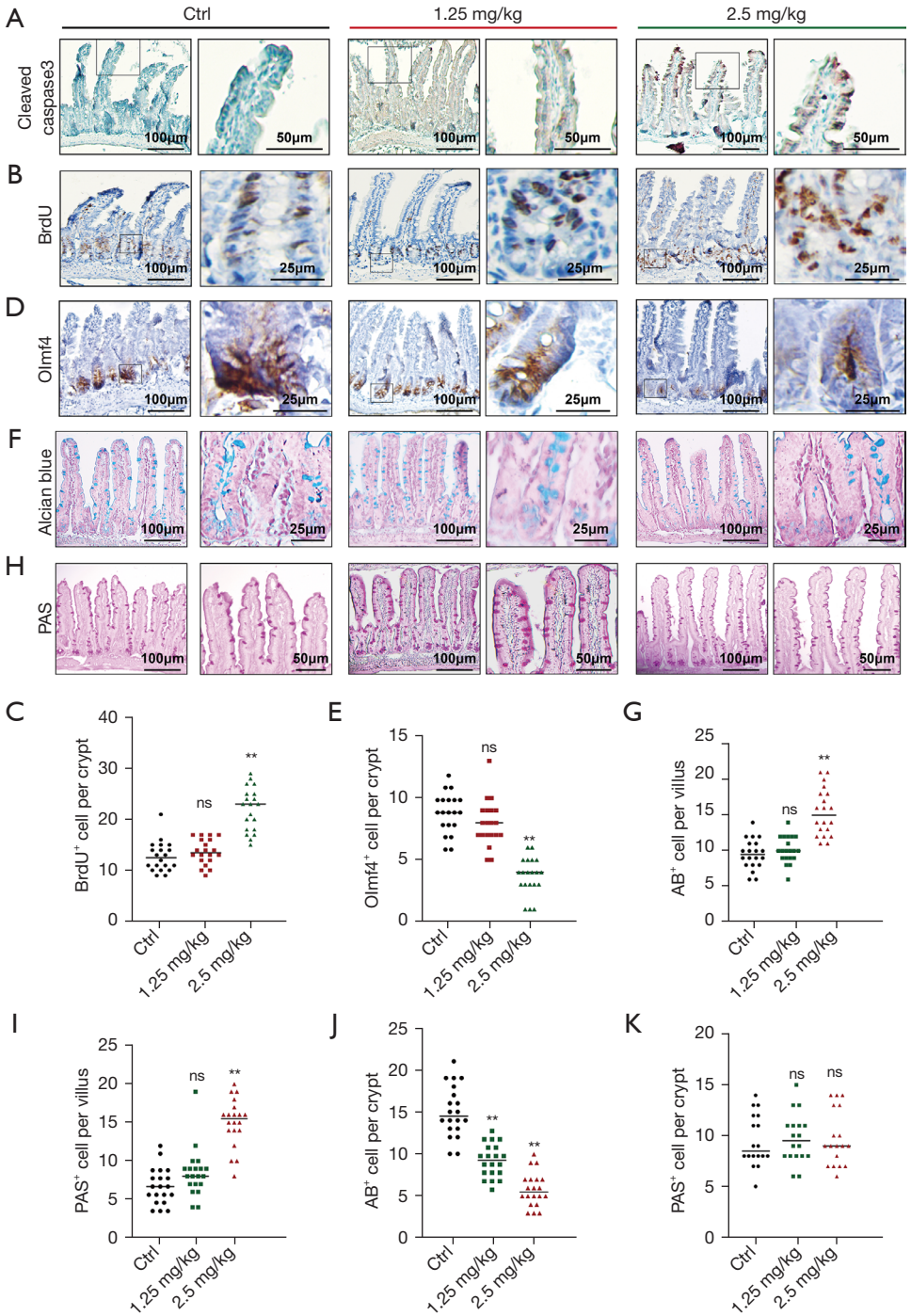

Figure 4 LCCDEs caused significant changes of ISCs' proliferation and differentiation pattern. (A) Representative images of cleaved-caspase-3 IHC staining between control mice and LCCDEs-treated mice. (B) Representative images and (C) quantification of BrdU$^+$ proliferating cryptal epithelial cells in control and LCCDEs-treated mice (n=3 per group). (D) Representative pictures and (E) quantification of Olmf4$^+$ ISCs in different groups (n=3 per group). (F) Representative pictures and (G,H) quantification of Alcian blue staining of villus and crypt in control and LCCDEs-treated mice (n=5 each group). (I) Representative picture and (J,K) quantification of PAS positive cells in villus and crypt in control and LCCDEs-treated mice (n=5 each group). **, P<0.01; ns, not significant. ISCs, intestinal stem cells; IHC, immunohistochemistry; BrdU, 5-bromo-2'-deoxyuridine; Olmf4, Olfactomedin 4; PAS, periodic acid-Schiff; AB, Alcian blue.

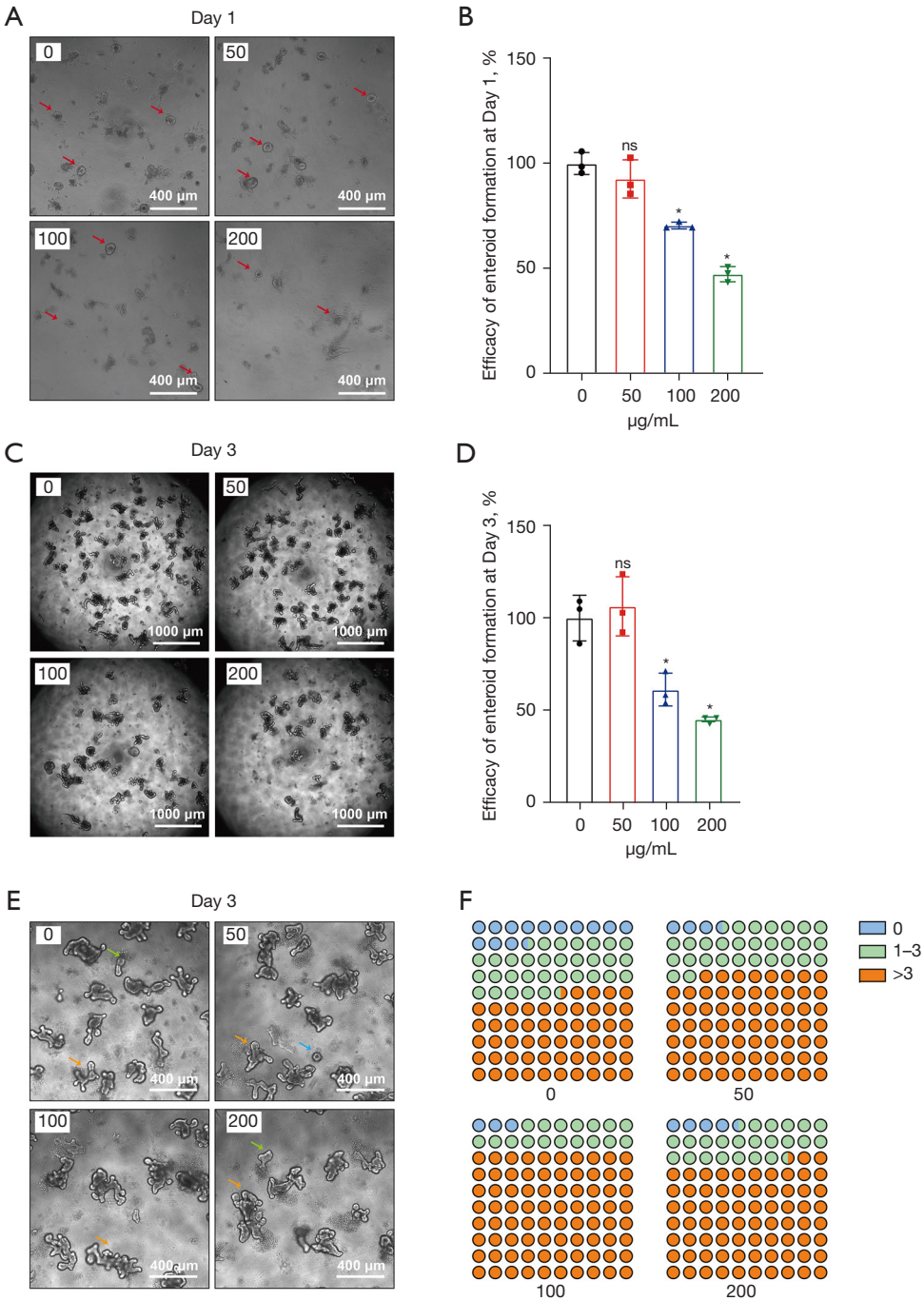

Figure 5 LCCDEs inhibited the formation and growth of small intestinal organoids *in vitro*. (A,B) Higher concentrations of LCCDEs caused more significant impairment of small intestinal organoid proliferation at day 1. Red arrows indicated the formed enteroids at day 1. (C,D) Higher concentration of LCCDEs was accompanied by greater impairment of small intestinal organoid proliferation at day 3. (E,F) LCCDEs had no impairment on the differentiation of enteroids. The concentrations of LCCDEs were 50, 100, and 200 μg/mL respectively (n=4). Buds of enteroids were counted and the percentage was shown in dot matrix (0: enteroids had no buds; 1–3, enteroids had 1–3 buds; >3, enteroids had more than 3 buds). *, P<0.05; ns, not significant. LCCDEs, lung cancer cell derived exosomes.

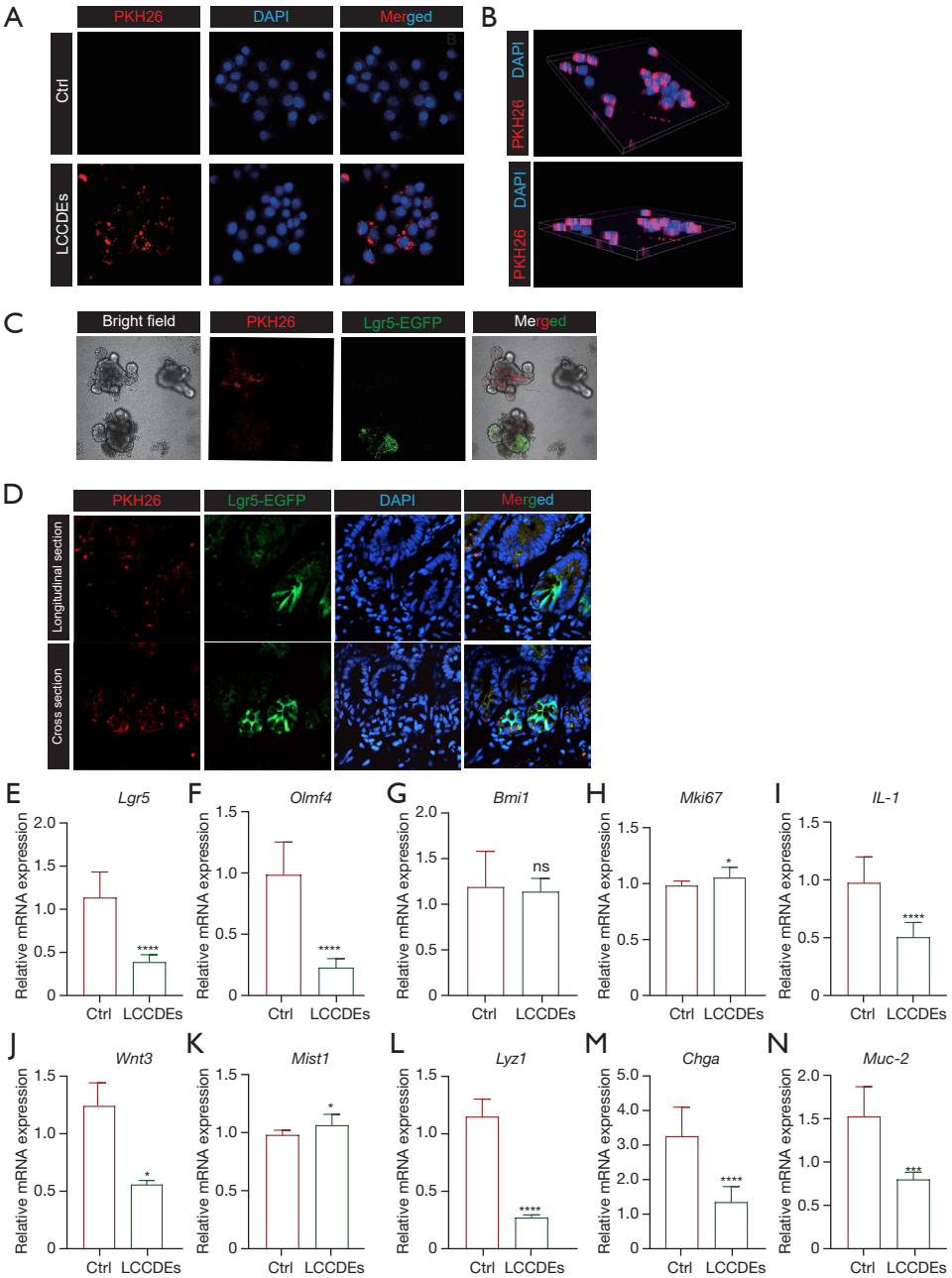

Figure 6 LCCDEs negatively reshaped the niche of ISCs. (A,B) PKH26-positive LCCDEs were absorbed by IEC-6 cells. IEC-6 cells were stained with DAPI to visualize nuclei, and PKH26 (a red fluorescent dye) was used to label LCCDEs. (C) PKH26 labeled LCCDEs were absorbed by enteoirds derived from Lgr5-EGFP mice. PKH26 staining was used to label LCCDEs, and the green fluorescence indicated EGFP positive Lgr5^{+} ISCs from Lgr5-EGFP mice derived enteroids. (D) Representative longitudinal section and cross section images of intestinal crypts after administration of PKH26 labeled LCCDEs. PKH26 was used to label LCCDEs, and the green fluorescence indicates intestinal stem cells from Lgr5-EGFP mice. (E-N) Relative mRNA changes of *Lgr5*, *Olmf4*, *Bmi1*, *Mki67*, *IL-1*, *Wnt3*, *Mist1*, *Lyz1*, *Chga*, *Muc-2* in small intestines of LCCDEs-treated mice (n=3 per group). *, P<0.05; ***, P<0.001; ****, P<0.0001; ns, not significant. LCCDEs, lung cancer cell derived exosomes; ISCs, intestinal stem cells; IEC-6, intestinal epithelial cell line 6; DAPI, 4',6-diamidino-2-phenylindole; *Lgr5*, Leucine rich repeat containing G protein coupled receptor 5; *Olmf4*, Olfactomedin 4; *Bmi1*, B cell specific Moloney murine leukemia virus integration site 1; *Mki67*, marker of proliferation Ki-67; *IL-1*, interleukin 1; *Wnt3*, wingless-type MMTV integration site family, member 3; *Mist1*, basic helix-loop-helix family, member a15; *Lyz1*, lysozyme 1; *Chga*, chromogranin A; *Muc-2*, mucin2.

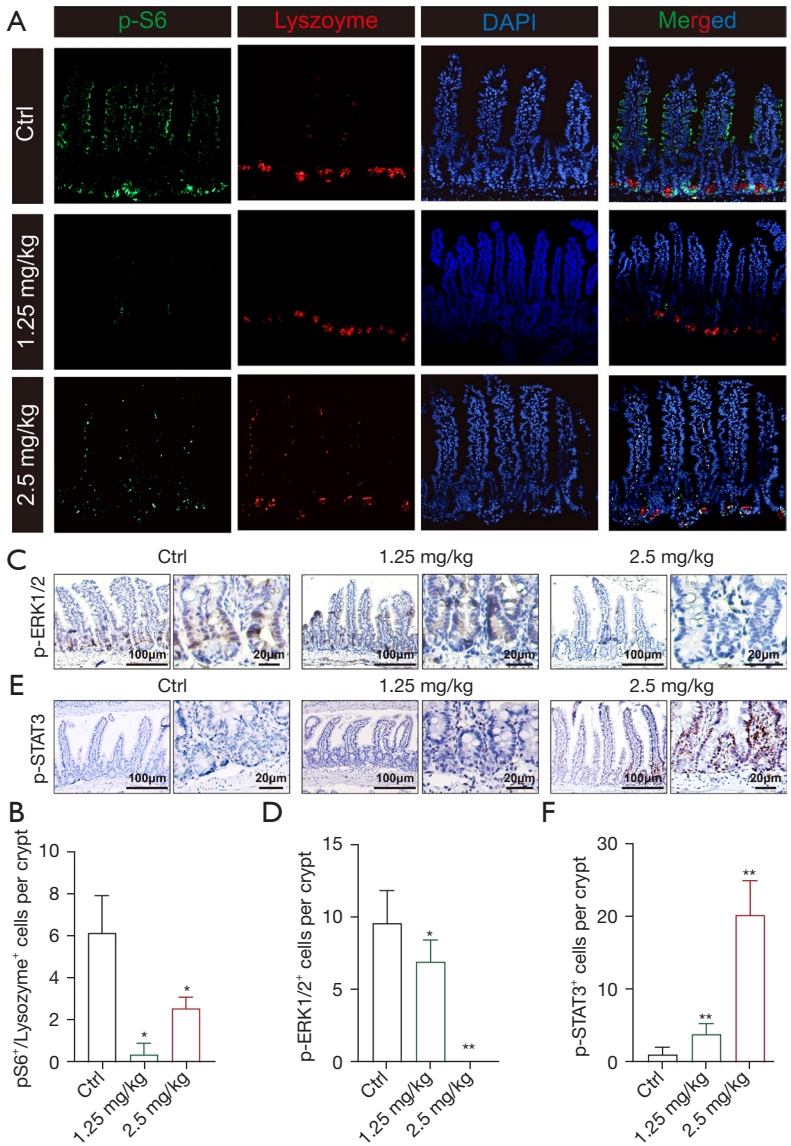

Figure 7 LCCDEs inhibited the activity of mTORC1, ERK and STAT3 signaling pathways. (A) Representative immunofluorescent images of p-S6 and lysozyme. (B) Quantification of pS6$^+$/Lysozyme$^+$ Paneth cells in control mice and LCCDEs treated mice (n=5 per group). (C) Representative images of p-ERK1/2 positive cells and (D) the number of p-ERK1/2 positive cryptal epithelial cells were decreased after the treatment of LCCDEs (n=5 per group). (E) Representative images of p-STAT3 positive cells and (F) statistical analysis of p-STAT3 positive cryptal epithelial cells (n=5 each group). *, P<0.05; **, P<0.01. LCCDEs, lung cancer cell derived exosomes; p-S6, phospho-S6; p-ERK1/2, phospho-extracellular regulated protein kinases 1/2; p-STAT3, phospho-signal transducer and activator of transcription 3.

niche-associated genes. Therefore, we inferred that the phenotype caused by LCCDEs in the small intestine could be attributed to its negative influence on ISCs.

Here, we demonstrated how LCCDEs impaired gross condition and intestinal function in mice, and a similar association between lung cancer and weight loss has also been reported by other researchers. They explained CAC from different perspectives. First, inflammatory mediators, such as tumor necrosis factor-alpha (TNFα), interleukin-6 (IL-6), and lipocalin-2 (LCN2), are the major drivers of CAC, which results in changes in the secretory profile of cancer-associated fibroblasts (CAFs) (26-28). Second, many mediators that are necessary for tissue homeostasis, especially components of the GDF15-GFRAL pathway,

are promising targets for overcoming CAC (29). Third, metabolic products of cancer cells can induce diurnal and metabolic changes in the liver. Finally, some studies revealed through tumor genomics and plasma proteomics analysis the key factors linking cancer and weight loss. For instance, it has been reported that in primary non-small cell lung cancer (NSCLC) patients, altered tumor genomic profiles and plasma proteomic profiles are strongly associated with cachexia and can decrease body weight and lead to loss of skeletal muscle content (30). However, we wondered whether other unmentioned factors, in addition to mediators of inflammation and tissue homeostasis and metabolic products, are related to lung cancer-induced cachexia. Since exosomes are widely secreted by cancer cells, we proposed that LCCDEs, the most widely studied extracellular microvesicles, might be a potential circulating mediator that can circulate through the bloodstream to the GI tract and can thus be used as a promising target to alleviate CAC in lung cancer patients.

This study demonstrated that LCCDEs was a novel mediator of lung cancer-induced cachexia and revealed how LCCDEs impaired the function of ISCs. Due to the impairment of ISCs caused by circulating LCCDEs, the proliferation and differentiation of ISCs were greatly impaired. Dysfunction of ISCs was the major cause of shortened small intestines and loss of body weight *in vivo*, and it also hindered the formation and growth of enteroids *in vitro*. Similarly, many studies have reported that harmful factors derived from the tumor niche are able to flow through the blood circulation into the small intestine and play essential roles in multiple pathophysiological effects (31). Admittedly, LCCDEs-induced impairment of ISCs might not be the only mechanism that explains the observed phenotypes. For example, the gut microbiota is an important factor that shapes the GI microenvironment, which regulates the absorption capability of the small intestine and can even influence tumor progression and clinical therapeutic outcomes (32,33). Additionally, tumor-derived exosomes can influence intestinal function and cause an imbalance in glycometabolism by inhibiting the secretion of glucose-dependent insulinotropic peptide (GIP) and glucagon-like peptide-1 (GLP-1), which negatively regulate the proprotein convertase subtilisin/kexin type 1/3 (PCSK1/3) (34). Therefore, the present study provides new insights into the mechanisms of lung cancer-induced cachexia and provides a promising therapeutic target for limiting the accumulation of EVs.

Although our studies revealed a novel mechanism by which lung cancer and LCCDEs damage the small intestine, there are also several limitations that necessitate further exploration in the future. Despite the observed decrease in intestinal length and loss of ISCs, the intestinal epithelium seemed to be more proliferative, and villous height and cryptal depth increased in LCCDEs-treated mice, which seemed to contradict traditional perspectives (24,35-37). This inconsistency might be attributed to incomplete compensation by the epithelium. Such a difference between ISCs and the epithelium has also been reported by Lee *et al.* (38). They described a phenotype in SAMP1 mice in which the proliferation of the crypt-villus structure compensated for the dysfunction of ISCs or their niche. The renewal of the intestinal epithelium depends on both ISCs and transient amplification (TA) cells (37,39-43). In the case of loss or hypofunction of ISCs, TA cells might compensate for the renewal of epithelial cells, which might cause the observed inconsistency. Second, the exact molecules within LCCDEs that impair ISCs remain unclear. Exosomes contain a variety of messengers that have multiple functions in intracellular communication, such as DNA, mRNAs, miRNAs, circRNAs, proteins and bioactive lipids (44,45). Moreover, many harmful exosomal miRNAs, including miR-149-3p, miR-223 and miR-126a-3, impair the function of the intestine through multiple pathways. For instance, miR-149-3p packaged in exosomes could mediate intestinal inflammation by facilitating Th17 cell differentiation (46). miR-223 induces intestinal barrier dysfunction (47), and miR-126-3p damages intestinal cells through the PIK3R2 pathway (48). In addition, a decrease in the abundance of protective exosomal substances can also induce intestinal injury. For example, miR-142 restores the gut microenvironment to protect IECs (49), circEZH2_005, a significant circRNA, promotes $Lgr5^{+}$ ISCs proliferation to alleviate intestinal injury (50), and miR-129-5p inhibits intestinal epithelial ferroptosis mediated by ACSL4 (51). Other factors, such as miR-23a-3p, miR-378a-5p, and miR-22-3p, influence the intestine via different pathways (52-54). Hence, it is necessary to validate the specific contents of LCCDEs in the future.

Based on the phenotypes and mechanisms discussed in this study, the manipulation of LCCDEs could be a promising method to partially overcome CAC and intestinal damage. For example, it might be useful to inhibit the secretion of LCCDEs. Enterotoxigenic *Bacteroides fragilis* has been reported to interfere with exosome secretion *in vivo* (46). In addition, exosomes could be blocked before circulating into the small intestine. It has been shown

that some biomaterials can precisely identify harmful exosomes, including oncogenic exosomes. Oncogenic exosomes can be eliminated via molecules that specifically bind to positively charged mesoporous silica nanoparticles (MSNs) targeted to epidermal growth factor receptor (EGFR) (31). Microplastics and nanoplastics are widely used to affect intestinal barrier function (48). It might be helpful to upregulate the expression of exosomal miR-142, circEZH2_005, and miR-129-2-3p, which could provide an effective approach to protect intestinal function by remodeling the intestinal microenvironment. Gprc5a signaling and the TIMELESS-mediated cellular senescence pathway have been proven to be involved in this process (49,50,55). In our study, GW4869 was shown to ameliorate the damage caused by LCCDEs *in vitro*.

Conclusions

Overall, in this study, we reported that lung cancer cell derived conditioned medium, and purified LCCDEs in particular, could impair the physiology of the small intestine, and we revealed that the major cause of this phenomenon was the ability of LCCDEs to impair ISCs and change the composition of the ISCs niche. This work provides a new explanation for CAC, and these findings suggest that reducing the level of LCCDEs might be a valuable therapeutic approach for the clinical treatment of CAC in lung cancer patients.

Acknowledgments

We thank all the members in Dr. Liu's laboratory for the critical reading and contributive suggestions during the preparation of this manuscript.

Footnote

Reporting Checklist: The authors have completed the ARRIVE reporting checklist. Available at https://tlcr.amegroups.com/article/view/10.21037/tlcr-24-758/rc

Data Sharing Statement: Available at https://tlcr.amegroups.com/article/view/10.21037/tlcr-24-758/dss

Peer Review File: Available at https://tlcr.amegroups.com/article/view/10.21037/tlcr-24-758/prf

Funding: This work was supported by Science and Technology Department of Sichuan Province (2020YJ0458, 2023YFS0089), Sichuan Cancer Hospital (YBR2019003), Guangdong Association of Clinical Trials (GACT)/Chinese Thoracic Oncology Group (CTONG), Guangdong Provincial Key Lab of Translational Medicine in Lung Cancer (YC20210105) and 2022CSCO key program (Y-2021AST/zd-0119), Wu Jieping Medical Foundation (320.6750.2021-22-21) and Beijing Life Oasis Public Service Center (ilvzhou-2023-001).

Conflicts of Interest: All authors have completed the ICMJE uniform disclosure form (available at https://tlcr.amegroups.com/article/view/10.21037/tlcr-24-758/coif). The authors have no conflicts of interest to declare.

Ethical Statement: The authors are accountable for all aspects of the work in ensuring that questions related to the accuracy or integrity of any part of the work are appropriately investigated and resolved. The animal experiments were conducted in accordance with the guidelines of the National Institutes of Health (NIH) "Guide for the Care and Use of Laboratory Animals (8th edition)", and all the experimental procedures were reviewed and approved by the Ethics Committee of Sichuan Cancer Hospital & Institute (No. SCCHEC-04-2023-01/8).

References

1. Bargetzi L, Brack C, Herrmann J, et al. Nutritional support during the hospital stay reduces mortality in patients with different types of cancers: secondary analysis of a prospective randomized trial. Ann Oncol 2021;32:1025-33.
2. Roeland EJ, Bohlke K, Baracos VE, et al. Management of Cancer Cachexia: ASCO Guideline. J Clin Oncol 2020;38:2438-53.
3. Ferrer M, Anthony TG, Ayres JS, et al. Cachexia: A systemic consequence of progressive, unresolved disease.

Cell 2023;186:1824-45.
4. He J, Jiang P, Ma L, et al. Intravenous immunoglobulin protects the integrity of the intestinal epithelial barrier and inhibits ferroptosis induced by radiation exposure by activating the mTOR pathway. Int Immunopharmacol 2024;131:111908.
5. Beumer J, Clevers H. Cell fate specification and differentiation in the adult mammalian intestine. Nat Rev Mol Cell Biol 2021;22:39-53.
6. Wu N, Sun H, Zhao X, et al. MAP3K2-regulated intestinal stromal cells define a distinct stem cell niche. Nature 2021;592:606-10.
7. Huang L, Xu Z, Lei X, et al. Paneth cell-derived iNOS is required to maintain homeostasis in the intestinal stem cell niche. J Transl Med 2023;21:852.
8. Chrisnandy A, Blondel D, Rezakhani S, et al. Synthetic dynamic hydrogels promote degradation-independent in vitro organogenesis. Nat Mater 2022;21:479-87.
9. Kalluri R, LeBleu VS. The biology, function, and biomedical applications of exosomes. Science 2020;367:eaau6977.
10. Thakur A, Parra DC, Motallebnejad P, et al. Exosomes: Small vesicles with big roles in cancer, vaccine development, and therapeutics. Bioact Mater 2022;10:281-94.
11. Cheng W, Wang K, Zhao Z, et al. Exosomes-mediated Transfer of miR-125a/b in Cell-to-cell Communication: A Novel Mechanism of Genetic Exchange in the Intestinal Microenvironment. Theranostics 2020;10:7561-80.
12. Ocansey DKW, Zhang L, Wang Y, et al. Exosome-mediated effects and applications in inflammatory bowel disease. Biol Rev Camb Philos Soc 2020;95:1287-307.
13. Oszvald Á, Szvicsek Z, Sándor GO, et al. Extracellular vesicles transmit epithelial growth factor activity in the intestinal stem cell niche. Stem Cells 2020;38:291-300.
14. Hosseini R, Asef-Kabiri L, Yousefi H, et al. The roles of tumor-derived exosomes in altered differentiation, maturation and function of dendritic cells. Mol Cancer 2021;20:83.
15. Ahmadi M, Rezaie J. Tumor cells derived-exosomes as angiogenenic agents: possible therapeutic implications. J Transl Med 2020;18:249.
16. Kumar MA, Baba SK, Sadida HQ, et al. Extracellular vesicles as tools and targets in therapy for diseases. Signal Transduct Target Ther 2024;9:27.
17. Jiang C, Zhang N, Hu X, et al. Tumor-associated exosomes promote lung cancer metastasis through multiple mechanisms. Mol Cancer 2021;20:117.
18. Chen R, Xu X, Qian Z, et al. The biological functions and clinical applications of exosomes in lung cancer. Cell Mol Life Sci 2019;76:4613-33.
19. Wortzel I, Dror S, Kenific CM, et al. Exosome-Mediated Metastasis: Communication from a Distance. Dev Cell 2019;49:347-60.
20. Anastasi F, Botto A, Immordino B, et al. Proteomics analysis of circulating small extracellular vesicles: Focus on the contribution of EVs to tumor metabolism. Cytokine Growth Factor Rev 2023;73:3-19.
21. Lei Y, Fei X, Ding Y, et al. Simultaneous subset tracing and miRNA profiling of tumor-derived exosomes via dual-surface-protein orthogonal barcoding. Sci Adv 2023;9:eadi1556.
22. Ahmadian S, Jafari N, Tamadon A, et al. Different storage and freezing protocols for extracellular vesicles: a systematic review. Stem Cell Res Ther 2024;15:453.
23. Zhang X, Borg EGF, Liaci AM, et al. A novel three step protocol to isolate extracellular vesicles from plasma or cell culture medium with both high yield and purity. J Extracell Vesicles 2020;9:1791450.
24. Ohta Y, Fujii M, Takahashi S, et al. Cell-matrix interface regulates dormancy in human colon cancer stem cells. Nature 2022;608:784-94.
25. Liao Y, Chen X, Miller-Little W, et al. The Ras GTPase-activating-like protein IQGAP1 bridges Gasdermin D to the ESCRT system to promote IL-1β release via exosomes. EMBO J 2023;42:e110780.
26. Setiawan T, Sari IN, Wijaya YT, et al. Cancer cachexia: molecular mechanisms and treatment strategies. J Hematol Oncol 2023;16:54.
27. Sun Q, van de Lisdonk D, Ferrer M, et al. Area postrema neurons mediate interleukin-6 function in cancer cachexia. Nat Commun 2024;15:4682.
28. Liu X, Li S, Cui Q, et al. Activation of GPR81 by lactate drives tumour-induced cachexia. Nat Metab 2024;6:708-23.
29. Suriben R, Chen M, Higbee J, et al. Antibody-mediated inhibition of GDF15-GFRAL activity reverses cancer cachexia in mice. Nat Med 2020;26:1264-70.
30. Al-Sawaf O, Weiss J, Skrzypski M, et al. Body composition and lung cancer-associated cachexia in TRACERx. Nat Med 2023;29:846-58.
31. Xie X, Nie H, Zhou Y, et al. Eliminating blood oncogenic exosomes into the small intestine with aptamer-functionalized nanoparticles. Nat Commun 2019;10:5476.
32. Teng Y, Ren Y, Sayed M, et al. Plant-Derived Exosomal MicroRNAs Shape the Gut Microbiota. Cell Host Microbe 2018;24:637-652.e8.

33. El Tekle G, Garrett WS. Bacteria in cancer initiation, promotion and progression. Nat Rev Cancer 2023;23:600-18.
34. Zhang Y, Huang S, Li P, et al. Pancreatic cancer-derived exosomes suppress the production of GIP and GLP-1 from STC-1 cells in vitro by down-regulating the PCSK1/3. Cancer Lett 2018;431:190-200.
35. Bonis V, Rossell C, Gehart H. The Intestinal Epithelium - Fluid Fate and Rigid Structure From Crypt Bottom to Villus Tip. Front Cell Dev Biol 2021;9:661931.
36. Konopka A, Gawin K, Barszcz M. Hedgehog Signalling Pathway and Its Role in Shaping the Architecture of Intestinal Epithelium. Int J Mol Sci 2024;25:12007.
37. Xiang J, Guo J, Zhang S, et al. A stromal lineage maintains crypt structure and villus homeostasis in the intestinal stem cell niche. BMC Biol 2023;21:169.
38. Lee C, Hong SN, Kim ER, et al. Depletion of Intestinal Stem Cell Niche Factors Contributes to the Alteration of Epithelial Differentiation in SAMP1/YitFcsJ Mice With Crohn Disease-Like Ileitis. Inflamm Bowel Dis 2021;27:667-76.
39. Li Y, Zhang M, Ma X, et al. Tuft cells promote human intestinal epithelium regeneration as reserve stem cells after irradiation. Cell Regen 2024;13:28.
40. Wang Y, Song W, Yu S, et al. Intestinal cellular heterogeneity and disease development revealed by single-cell technology. Cell Regen 2022;11:26.
41. Kim JE, Fei L, Yin WC, et al. Single cell and genetic analyses reveal conserved populations and signaling mechanisms of gastrointestinal stromal niches. Nat Commun 2020;11:334.
42. Liu Y, Xiong X, Chen YG. Dedifferentiation: the return road to repair the intestinal epithelium. Cell Regen 2020;9:2.
43. Yeung TM, Chia LA, Kosinski CM, et al. Regulation of self-renewal and differentiation by the intestinal stem cell niche. Cell Mol Life Sci 2011;68:2513-23.
44. Paskeh MDA, Entezari M, Mirzaei S, et al. Emerging role of exosomes in cancer progression and tumor microenvironment remodeling. J Hematol Oncol 2022;15:83.
45. Yang E, Wang X, Gong Z, et al. Exosome-mediated metabolic reprogramming: the emerging role in tumor microenvironment remodeling and its influence on cancer progression. Signal Transduct Target Ther 2020;5:242.
46. Cao Y, Wang Z, Yan Y, et al. Enterotoxigenic Bacteroidesfragilis Promotes Intestinal Inflammation and Malignancy by Inhibiting Exosome-Packaged miR-149-3p. Gastroenterology 2021;161:1552-1566.e12.
47. Chang X, Song YH, Xia T, et al. Macrophage-derived exosomes promote intestinal mucosal barrier dysfunction in inflammatory bowel disease by regulating TMIGD1 via mircroRNA-223. Int Immunopharmacol 2023;121:110447.
48. Huang Z, Weng Y, Shen Q, et al. Nano- and micro-polystyrene plastics interfered the gut barrier function mediated by exosomal miRNAs in rats. Environ Pollut 2023;335:122275.
49. Li H, Zhao S, Jiang M, et al. Biomodified Extracellular Vesicles Remodel the Intestinal Microenvironment to Overcome Radiation Enteritis. ACS Nano 2023;17:14079-98.
50. Zhang W, Zhou B, Yang X, et al. Exosomal circEZH2_005, an intestinal injury biomarker, alleviates intestinal ischemia/reperfusion injury by mediating Gprc5a signaling. Nat Commun 2023;14:5437.
51. Wei Z, Hang S, Wiredu Ocansey DK, et al. Human umbilical cord mesenchymal stem cells derived exosome shuttling mir-129-5p attenuates inflammatory bowel disease by inhibiting ferroptosis. J Nanobiotechnology 2023;21:188.
52. Yang J, Zheng XG, Wu YL, et al. Intestinal epithelial cell-derived exosomes package microRNA-23a-3p alleviate gut damage after ischemia/reperfusion via targeting MAP4K4. Biomed Pharmacother 2022;149:112810.
53. Cai X, Zhang ZY, Yuan JT, et al. hucMSC-derived exosomes attenuate colitis by regulating macrophage pyroptosis via the miR-378a-5p/NLRP3 axis. Stem Cell Res Ther 2021;12:416.
54. Jiang R, Lönnerdal B. Milk-Derived miR-22-3p Promotes Proliferation of Human Intestinal Epithelial Cells (HIECs) by Regulating Gene Expression. Nutrients 2022;14:4901.
55. Wei S, Wu X, Chen M, et al. Exosomal-miR-129-2-3p derived from Fusobacterium nucleatum-infected intestinal epithelial cells promotes experimental colitis through regulating TIMELESS-mediated cellular senescence pathway. Gut Microbes 2023;15:2240035.

Cite this article as: Wang K, Xu L, Feng J, Wang S, Wang X, Zou J, Xu Z, Huang L, Jiang W, Zhou J, Lei X, Liu D. Circulating lung cancer exosomes damage the niche of intestinal stem cells. Transl Lung Cancer Res 2025;14(3):718-735. doi: 10.21037/tlcr-24-758